Preprint typeset using LaTeX style emulateapj v. 04/17/13

THE EFFECTS OF TELLURIC LINES IN RADIAL VELOCITY SEARCHES FOR PLANETS WITH IODINE CELLS AS CALIBRATORS[1]

Sharon Xuesong Wang (王雪凇)[2,3], Jason T. Wright[2,3], Chad Bender[2,3], Andrew W. Howard[4], Geoffrey W. Marcy[5], Howard Isaacson[5], and Suvrath Mahadevan[2,3]

ABSTRACT

Tellurics are bad and you really don't want them. Here's why and how to get rid of them.

Subject headings: instrumentation

1. INTRODUCTION

The first exoplanets around main-sequence stars were discovered by the radial velocity (RV) method, where precise Doppler spectroscopy measures the wavelength shift of the host stars induced by the gravitational pull of the planets (Campbell et al. 1988; Latham et al. 1989; Hatzes & Cochran 1993; Mayor & Queloz 1995; Butler & Marcy 1996). Since then, the RV method has discovered hundreds of planetary systems (see exoplanets.org; Han et al. 2014) and contributed to numerous confirmation and characterization of exoplanets discovered by the transit method (e.g., for *Kepler* follow-up observations; Marcy et al. 2014).

The current best RV precision is around 1 m/s (Fischer et al. 2016), attainable via two wavelength calibration methods in the optical band: ThAr lamp emission line calibration (e.g., ELODIE and HARPS; Baranne et al. 1996; Mayor et al. 2003; ∼400-690 nm) and iodine cell absorption line calibration (e.g., Keck/HIRES and Magellan/PFS; Butler et al. 1996; Crane et al. 2010; ∼500-620 nm). The major obstacles for achieving a higher RV precision are: stellar activity induced RV signals, instrumental effects, telluric contamination, and limitation in data analysis (Fischer et al. 2016).

Traditionally, telluric contamination is not considered as problematic for precise RV in the optical. It is certainly a sever source of spectral contamination and a bottleneck for achieving higher RV precision in the near infra-red (NIR) region (e.g., Bean et al. 2010), where a large number of deep water and methane lines reside. However, there is only a small wavelength range in the optical that has deep telluric lines, and typically such regions are simply thrown out for the purpose of precise RV analysis, either by giving them zero weights in the cross correlation masks (for ThAr calibrated spectra, e.g., Pepe et al. 2002) or flagging them as bad pixels (for iodine calibrated spectra, e.g., for Keck/HIRES).

Recently, the works by Artigau et al. (2014) and Cunha et al. (2014) have characterized and mitigated the effects of telluric contamination in the precise RV data taken by the ThAr-calibrated HARPS-S. Cunha et al. (2014) focuses on the issues with "micro-telluric" lines (shallow telluric absorption lines with < 1-3% depths), which are recognized for the first time. Cunha et al. (2014) fit and then divide out the telluric lines in the observed spectra using synthetic telluric spectra generated by the LBLRTM package (Line-By-Line Radiative Transfer Model, Clough et al. 1992; with line lists from HIgh-resolution TRANsmission molecular absorption database, or HITRAN, Rothman et al. 2013) and also TAPAS (Bertaux et al. 2014), which is a more user-friendly but less flexible package wrapper using LBLRTM. They concluded that the micro-tellurics have an impact (defined as RMS of difference between RVs before and after micro-telluric removal) of ∼10-20 cm/s for G stars observed with low to moderate air masses, but the impact can be substantial in some cases to up to ∼0.5-1 m/s.

Artigau et al. (2014) uses principal component analysis (PCA) to empirically correct for telluric lines in HARPS-S data (both micro-tellurics and the deep lines in the ∼630 nm region), and combined PCA with rejection masking, they reduced the RV RMS by ∼20 cm/s (and more significantly for the ∼630 nm region). More recently, Sithajan et al. (2016) characterized the effects of telluric contamination and effectiveness of some typical remedies (masking and modeling) for emission line-calibarated spectra for the optical, broad optical (300-900 nm), and NIR. Their conclusion for the optical region is similar to the results in Artigau et al. (2014) and Cunha et al. (2014).

This paper characterizes and corrects for the adverse effects of telluric contamination under the context of iodine-calibrated precise RV, especially for the micro-telluric lines. ZZZ We first describe our methodology for characterizing the effects of tellurics in, then... ZZZ

2. CHARACTERIZATION OF THE IMPACTS OF MICRO-TELLURICS ON RV PRECISION VIA SIMULATION

To evaluate the impacts of micro-tellurics (referred to often simply as "tellurics" below), we performed end-to-end simulation of Keck/HIRES data and analysis process on RV standard stars in order to isolate error sources. We use Keck/HIRES data to for our study because Keck has the highest RV precision among all iodine-calibrated

[1] Based on observations observations obtained at the Keck Observatory, which is operated by the University of California. The Keck Observatory was made possible by the generous financial support of the W. M. Keck Foundation.

[2] Department of Astronomy and Astrophysics, 525 Davey Laboratory, The Pennsylvania State University, University Park, PA 16802, USA; Send correspondence to xxw131@psu.edu and jtwright@astro.psu.edu

[3] Center for Exoplanets and Habitable Worlds, 525 Davey Laboratory, The Pennsylvania State University, University Park, PA 16802, USA

[4] Hawaii, USA

[5] Department of Astronomy, University of California, Berkeley, CA 94720, USA

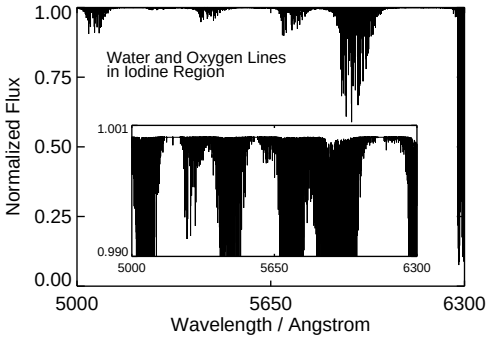

FIG. 1.— Telluric lines in the iodine region are mostly shallow water lines, with some moderately deep water lines near 5900Å and very deep oxygen lines near 6300Å. The insert plot is showing the pervasiveness of micro-telluric lines, i.e. ⩽1–3% in depths.

spectrometers, and it also has long observing baselines on a number of RV standard stars. RV standard stars are bright and quiet stars which do not host known planets, and thus exhibit the smallest RV variation in both short term and long term. Their data are often good diagnostic tools for identifying RV systematics. For our study, we used and simulated Keck/HIRES RV spectra on two standard stars, σ Draconis (HD 185144) and τ Ceti (HD 10700), which are benchmark classics in precise RV work.

HD 185144 (spectral type G9V, per Simbad) has 712 Keck/HIRES observations, with RV RMS = 2.57 m/s, and it has a relatively small barycentric velocity (often referred to as the barycentric velocity correction, or BC) span, $[-4.7,\ 4.6]$ km/s, because it is near the north ecliptic pole. HD 10700 (spectral type G8.5V) has 623 observations, with RMS = 3.05 m/s, and its BC span is $[-27.8,\ 26.8]$ km/s. The RV RMS numbers quoted here come from reductions using our version of CPS Doppler pipeline, and they are larger than the RMS values from the most up-to-date CPS pipeline due to some recent improvements in the CPS version. The most recent CPS inventory (as of April 2016) also has a few new observations on these two stars.

We describe how we simulated our data and used them to characterize the impacts of tellurics in Section 2.1, and then lay out our results in Section 2.2.

2.1. *Methodology of the Simulation*

The overall strategy is to bring out the effects of telluric contamination by comparing the extracted RVs from pairs of simulated observations: one with telluric absorption, and the other one in the pair without. For example, for HD 185144, we simulated two spectra for each of the 712 real observed spectrum. We then had two sets of simulated observations, one free of tellurics and one contaminated with tellurics. Next we ran the Doppler code on each set of 712 spectra to extract RVs from them, and for the set with tellurics we used telluric-contaminated DSST and a telluric-free DSST for the telluric-free spectra.

Below is our recipe for simulating Keck/HIRES spectra and DSSTs:

1. Generate a synthetic spectrum for the target star using Spectroscopy Made Easy (SME; Valenti & Piskunov 1996; Valenti & Fischer 2005; the SME spectra are kindly provided by Jason Curtis). We refer to this spectrum as the input synthetic spectrum or the SME spectrum.

2. Based on the SME spectrum, generate a deconcolved stellar spectral template (DSST) for the target star. First, we redshift the SME spectrum so that it has the same barycentric velocity as the real DSST of the target star. Then we break the SME spectrum into chunks as defined by the real DSST (an IDL structure) of this target star.

3. Run TERRASPEC (Bender et al. 2012), a versatile software for synthesizing telluric spectrum (it is a wrapper around the HITRAN line list (Rothman et al. 2013) and the LBLRTM package (Clough et al. 1992), developed by Chad Bender, who provided crucial help in this work for using TERRASPEC), to generate a telluric absorption spectrum using a typical Mauna Kea atmospheric condition in the summer, with precipitable water vapor (pwv) 1 mm[6], and oxygen column density that is consistent with the altitude of the real DSST observation. We multiply this synthetic telluric spectrum with the SME spectrum to make a telluric-contaminated DSST.

4. Loop through each real observed spectrum of the target star, and simulate a pair of observations following this recipe:

   (a) Shift the SME spectrum to have the same barycentric velocity as the star at the epoch of the real observation (i.e., assuming intrinsic stellar velocity is zero).

   (b) Generate a continuous wavelength solution for each echelle order based on the best-fit wavelength solution for the real spectrum.

   (c) Re-sample the SME spectrum and the iodine atlas onto a wavelength grid that is four times finer than the wavelength solution grid. Multiply the stellar spectrum with the iodine atlas.

   (d) To add telluric contamination: multiply the simulated spectrum with a telluric absorption spectrum generated with TERRASPEC, again for typical Mauna Kea summer, with pwv = 1 mm, and oxygen column density that is consistent with the altitude of the real observation.

   (e) Determine the IP for each echelle order with two options: (1) a single Gaussian with σ = 1.7 pixel, matching the Keck/HIRES resolution; (2) a sum-of-Gaussian IP derived using the average IPs for each echelle order. We will explain these two options later in the text.

   (f) Convolve each order of the stellar×iodine spectrum with the IP.

   (g) Fit for the blaze function for each order of the real observed spectrum with a third-order polynomial using the top 1% of the flux, and

[6] As reported at CFHT website.

multiply the simulated spectrum so that they have matching "blaze functions". This also ensures that the simulated spectrum has the same photon counts as the real one.

(h) Add photon noise according to Poisson statistics, when desired.

5. Generate a separate data log file for each set of simulated of observations under the same conditions (i.e., telluric choice, IP choice, photon-noise choice).

we first simulated spectra free of photon noise and with a simple single Gaussian IP for the spectrograph ($\sigma = 1.7$ pixels to match the Keck/HIRES resolution). When extracting RVs for such sets of simulated spectra, we fixed the IPs to the same as input and only fitted for three free parameters. This removes the errors induced by photon noise and uncertainties in IP fitting (which, after all, involves 12 additional free parameters). We then added the Poisson noise to the spectra, but still using simple and fixed IPs, to see how the effects will change in cases with limited-SNR (as opposed to infinite SNR). Next, we used complex IPs, the same ones as the best-fit sum-of-Gaussian IPs found for real spectra, and float the IP parameters when extracting RVs. For the simulated spectra with complex IPs, we extracted their RVs following exactly the same procedure for real observations, e.g., using IP initial guesses from solutions for real neighboring B star + iodine observations. The conditions and results of these three pairs of simulations are listed in Table 1, and also illustrated in Figure 2. These results show the impacts of telluric contamination on Keck/HIRES data, which is discussed in the following subsection.

2.2. *Results of the Simulation*

Figure 2 illustrates the effects of telluric contamination under different conditions. The top panels are RV differences between the simulated spectrum pairs with infinite SNR and perfectly known IPs, which might somewhat represent the capability of future precise RV instruments. These two plots highlight the net effects of telluric contamination: they cause large biases in RV estimates, which manifest as strong RV-BC correlations or trends. Clearly, the current statistical weighting or "vanking" procedure in the Doppler code is unable to fully correct these biases.

Interestingly, when we added in photon noise (middle panels of Figure 2), the effects of telluric contamination are washed out significantly. This is probably because photon noise induces a much bigger RV scatter than the micro-telluric lines. This is not surprising, given that the depths of these micro-telluric lines are often comparable to noise level. We are still investigating the exact reason of this "wash out".

When using complex IPs and fitting for IPs in RV extraction (bottom panels of Figure 2), the effects of telluric contamination are further washed out, as we are adding in more errors that are perhaps larger than telluric-induced ones. We can barely see any RV-BC correlation in the case of HD 185144 and only some in HD 10700.

The RV-BC correlations shown in Figure 2 will translate into spurious peaks in the periodograms of the target star, and such spurious peaks will have periods around a sidereal year and its harmonics. This is very damaging for the search of exoplanets in the Habitable Zone around Sun-like stars, which would have periods around 360 days. Besides these spurious signals, telluric contamination also causes increases in RV RMS. In all cases of telluric-free and telluric-contaminated simulation pairs, the RV RMS is larger for the telluric-contaminated case (Table 1). The RMS numbers written in Figure 2 represent the amount of RV RMS added (in quadrature) because of telluric contamination (again, the spectrum pairs are same-noise pairs – they only differ in terms of having or not having telluric lines). These numbers also represent an RV RMS floor set by the telluric contamination: for example, if we ignore tellurics in RV reduction, one would not achieve an RV precision of <0.6-0.7 m/s on G type stars using iodine cells as calibrators. This would compromise our ability to detect Earth or super-Earth exoplanets greatly (again, Earth 2.0 would have an RV amplitude of 0.08 m/s). In the next section, we discuss strategies to eliminate these adverse effects of telluric contamination for iodine-calibrated precise RV data.

2.3. *Remedies and Effectiveness*

There are several ways to remedy the adverse effects of telluric lines on RV precision and accuracy: masking, modeling, or a combination of both. Like the rest of this section, we focus our efforts on iodine-calibrated data. For ThAr-calibrated data, the current official HARPS pipeline masks deep telluric lines and abandons spectral orders that are heavily contaminated (Xavier Dumusque, private communication; Artigau et al. 2014). Sithajan et al. (2016) also discusses remedies and their effectiveness for ThAr-calibrated data in more band options including the near infrared.

2.3.1. *Masking is an ineffective solution*

The simplest solution is to mask out telluric lines in the spectrum, which means, in practice, locate the telluric-contaminated pixels and flag them as bad pixels in the observed spectrum so that the least-χ^2 fitter will ignore them. For Keck/HIRES or any iodine-calibrated RV reduction, this also means masking out the regions corresponding to locations of telluric lines in the deconvolved stellar reference spectrum – because the stellar reference spectrum was taken at a different BC, the telluric lines therein are shifted with respect to the ones in the epoch observation as we try to match up the stellar lines in observed and reference spectra. This double masking procedure is illustrated in Figure 3. This is done dynamically in the fitting process, in the sense that, for each iteration in the least-χ^2 minimization process, the contaminated pixels are located according to the current wavelength solution parameters in this fitting iteration. The wavelength solution changes from iteration to iteration, and thus the masked pixels can change too.

To investigate the effectiveness of masking, we performed RV extraction on simulated spectra with or without telluric lines injected and with or without masking (all with Poisson noise and complex IP to mimic real observations as much as possible). For stellar reference spectrum, we used the synthetic spectrum with telluric lines. The results are already listed in Table 1, but are

TABLE 1
List of Simulations

Simulation Conditions	Tellurics?	185144 RMS	10700 RMS	More Details in
No photon noise, simple, fixed IPs	No	0.62 m/s	1.95 m/s[c]	Section 2.2
	Yes	1.21 m/s	2.42 m/s[c]	top panels, Figure 2
Poisson noise, simple, fixed IPs[a]	No	2.11 m/s[c]	2.54 m/s[c]	Section 2.2
	Yes	2.12 m/s[c]	2.81 m/s[c]	middle panels, Figure 2
Poisson noise, complex, floating IPs,[a]	No	1.22 m/s	1.35 m/s	Section 2.2
	Yes	1.29 m/s	1.44 m/s	bottom panels, Figure 2
Poisson noise, complex, floating IPs, masking the telluric pixels[a]	No	1.27 m/s	1.43 m/s	Section 2.3.1
	Yes	1.27 m/s	1.43 m/s	Figure 3
				Table 2
Poisson noise, complex, floating IPs, modeling tellurics[b]	pwv = 0.5, 0.9	1.28, 1.22 m/s	1.32, 1.30 m/s	Section 2.4
	pwv = 1.0, 1.1	1.25, 1.23 m/s	1.33, 1.31 m/s	Figure 4

[a] With pairs of simulated spectra with or without tellurics and each pair has the same Poisson noise added.
[b] Telluric lines added with pwv = 1 mm, and we extracted RVs using pwv = 0.5, 0.9, 1.0, 1.1 mm to access how accurately/precisely one needs to model the tellurics.
[c] These simulations suffer from severe numerical and algorithmic errors for reasons not yet fully understood.

TABLE 2
Comparison of RV RMS between Simulations with or without Masking

HD 185144	HD 10700	Simulation Conditions
1.22 m/s	1.35 m/s	No tellurics
1.29 m/s	1.44 m/s	With tellurics
1.27 m/s	1.43 m/s	No tellurics; with masking
1.27 m/s	1.43 m/s	With tellurics; with masking

listed again in Table 2 for clear comparisons. In terms of improving RV precision or reducing RV RMS, masking is very ineffective. The additional errors it introduces diminish its merits. On the other hand, masking does improve the accuracy to some degree: for example, masking does remove the downward RV trend seen in HD 10700 data on the bottom right plot of Figure 2 in the BC range $[-3\times10^4,\ -2\times10^4]$ m/s. However, masking is an ineffective way to mitigate the effects of telluric contamination overall, especially since the RV errors and RV-BC trends are dominated by photon noise and algorithmic errors (and other types of errors too in real observations).

masking does not work? First of all, it complicates the χ^2 surface and "breaks" the L-M fitter. Due to the dynamic nature of the mask mentioned above, the degrees of freedom for fitting could change, because some telluric lines may shift in and out of this spectral chunk as the wavelength solution changes. This would make the fitter harder to converge or may create more local minima in which the fitter can get stuck, causing additional errors. A better fitter might solve the convergence problem, but it is hard to justify throwing away useful iodine and stellar content embedded in the masked pixels. Finally, to mask the telluric lines out, one needs to pick a flux threshold for the masks. This threshold must maintain a balance between masking too much (throwing away too much iodine and stellar information) and too little (leaving shallow telluric lines and line wings untreated). In our study, we have chosen a flux threshold of 0.3%, which means any pixel with telluric absorption deeper than 0.3% will be masked (reference telluric spectrum is generated by TERRASPEC at an zenith angel of 70°, meaning deep oxygen lines, and with pwv = 0.8 mm, a little more than typical Keck/HIRES humidity). This masks 11% of the spectral domain, which is quite substantial and is very damaging to the RV precision, but is almost the minimal amount of masking required to achieve some RV accuracy improvement as we found out by testing various masking depths.

We also applied telluric masking in RV reduction for real observations, and saw no improvement over RV precision or accuracy. This is because other effects dominate rather than tellurics, as mentioned above, such as photon and algorithmic errors and especially deconvolution errors in stellar reference spectrum.

To summarize, masking sounds like a simple solution to the problem of micro-telluric contamination, but it is actually complicated to implement (for iodine-calibrated RV reduction) and it is ineffective in terms of improving RV precision. We do not recommend masking as a remedy for treating micro-telluric lines in iodine-calibrated RV work. We believe the most effective way is to forward model telluric lines, and combine that with some "masking" for deep or troublesome telluric lines, which we discuss in the next subsection.

2.4. *How precisely does one need to model the tellurics?*

The other way is to incorporate telluric lines as part of the iodine RV forward modeling process, where water column density can either be from a priori knowledge or an additional free parameter. In principle, the oxygen column density can also be a free parameter, not because the amount of oxygen varies on a noticeable level, but just to allow some compensation for errors in atmospheric temperature and pressure profile and so on, in order to model the oxygen lines more precisely. We do not fit for oxygen in our simulation or treatment for real observations in this work for simplicity, and also because the chunks contaminated with oxygen lines are in the reddest part near 6300Å, where the amount of iodine and stellar contents are minimal anyway, and these chunks tend to be thrown away or heavily de-weighted in the final RV weighting process.

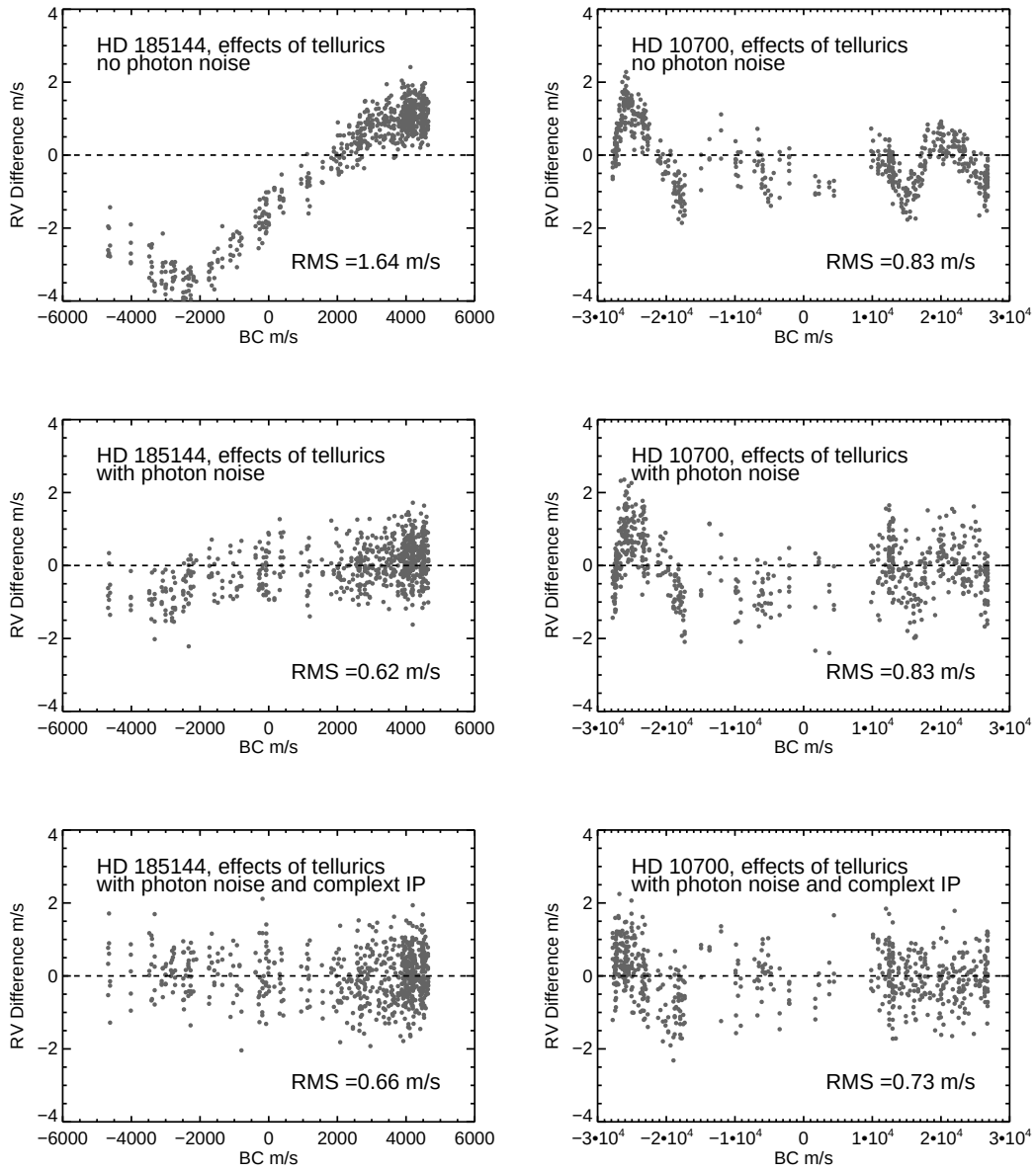

FIG. 2.— Effects of telluric lines manifested as correlation between RV and BC. Each point represents the difference in RV estimates for a pair of simulated spectra: one without telluric absorption, and one with telluric absorption on top of the stellar and iodine spectra. **Top 2 panels:** To isolate the effects of telluric lines, the simulated spectra used for this plot do not have Poisson noise added, and they have simple one-component Gaussian IPs which have fixed width and thus the IP parameters are all fixed to the true values in the RV extraction. **Middle 2 panels:** same as the top panels, but for simulated spectra with Poisson noise (same noise for the telluric and non-telluric spectrum pairs; and still the same simple IPs). **Bottom 2 panels:** same as above, but for simulated spectra with Poisson noise and complex IPs that are similar to the ones in actual observations. IP parameters are not fixed in this case, so the code is fitting 12 additional parameters for the IP on top of the 3 for wavelength solution and Doppler shift.

Modeling telluric absorption lines to high precision (below 1–2% RMS residual) can be a challenging task. There are several reasons for this: lab measurements of a large number of water lines are inaccurate, in terms of line depths, line positions, and line shapes; and these line properties can also be uncertain due to change or a lack of knowledge of the atmospheric conditions, such as wind, high line-of-sight variations (e.g., water vapor), and mixing uncertainties. For a summary of the state of the problem and paths forward recommended by the RV community, see Section 4.6 in Fischer et al. (2016). However, the goal here is not to model or remove the telluric lines perfectly, but to mitigate their impact on RV precision and accuracy as much as possible. A central question is: how well do we need to model telluric lines to reach a certain RV precision (Fischer et al. 2016)?

To answer this question under the context of iodine-calibrated RV, we performed RV extractions on the simulated HD 185144 data with telluric absorption (all with pwv = 1.0 mm, as described in Section 2.1), incorporating forward modeling of telluric lines with different levels of accuracy and using a stellar reference spectrum free of tellurics. The results are illustrated in Figure 4. All three simulations were run with simulated spectra of

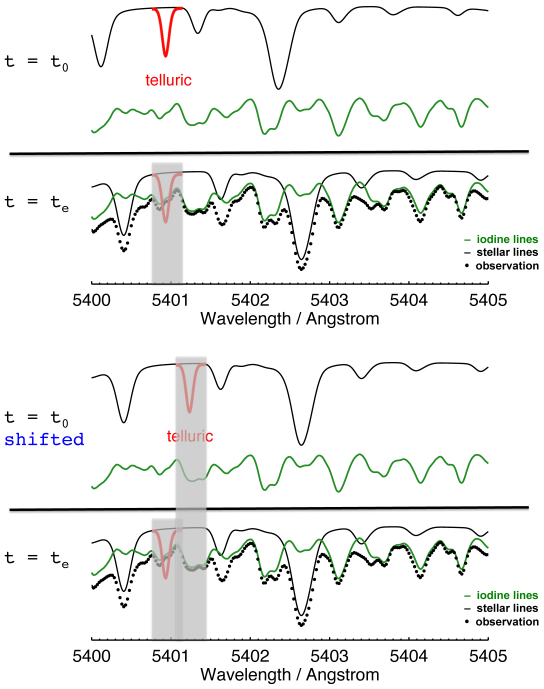

FIG. 3.— Illustration for how we mask telluric contaminated pixels. The top panel shows how we mask the telluric lines (red solid lines) in the epoch observation taken at $t = t_e$. The bottom panel shows why we also need to mask pixels associated with telluric lines in the deconvolved stellar reference spectrum taken at epoch $t = t_0$ and being shifted in order to model the observation.

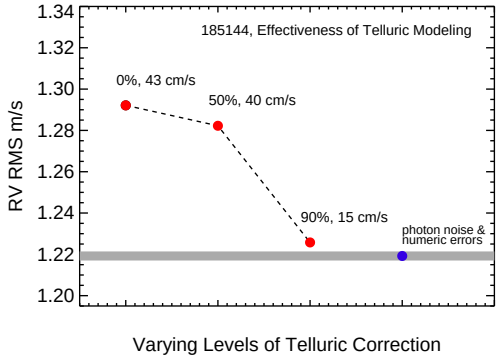

FIG. 4.— Improvements in RV RMS for different "level" of telluric modeling/removal. For example, the mid point labeled with "50%, 40 cm/s" means that if you model your telluric absorption lines to 50% of their original depths, the effects of the residual telluric absorption will add 40 cm/s in quadrature to your final RV RMS. The blue point marks the RV RMS for simulations with Poisson noise and complex IP on HD 185144, which represents the photon-limited RV precision (subject to additional numeric or algorithmic errors).

HD 185144 with pwv 1.0 mm, but the one labeled "0%" has no telluric modeling in the RV extraction, while the one labeled with "50%" has synthetic telluric lines with pwv 0.5 mm in the forward modeling process, and "90%" meaning using telluric model with pwv 0.9 mm. In addition, we also used telluric model with pwv 1.0 mm and 1.1 mm in the forward modeling, which produced similar RV RMS as the "90%" simulation with no visible RV-BC trends or correlations. A ∼90% modeling accuracy for the water lines would control the RV RMS contribution from tellurics to below 20 cm/s, which is near the target precision for the next generation RV spectrographs. This level of modeling precision is very easy to achieve in reality. However, it is worrisome that even 100% modeling with pwv 1.0 mm cannot eliminate the increase in RV RMS completely. To improve beyond 20 cm/s, we think that a next-generation Doppler code is needed.

One important point to notice is that the reason why the damage of 10% telluric modeling residual is controlled down to ⩽20 cm/s is the additional masking and weighting process in the Doppler code, i.e., "vanking". A combination of modeling (even only to 90% precision) and statistical weighting can effectively control the RV RMS introduced by tellurics to ⩽20 cm/s. Weighting plays a role in telluric contamination remedy because it is essentially performing some masking on the chunks that are badly contaminated by tellurics and/or have large modeling residuals, such as the ones near 6300Å with deep oxygen lines and little stellar or iodine content. Chunks with deep and numerous oxygen lines are normally thrown out completely, and other contaminated chunks which suffer from low precision will receive lower weights and thus cast a lower impact on the final precision and accuracy. In reality, we are using a combination of modeling and masking or weighting to tackle problem of telluric contamination, which we believe is the optimal solution for iodine-calibrated RVs.

2.4.1. *Treating telluric contamination in real observations*

The situation is much more complicated for real observations, because other noise sources enter the picture, some uncontrollable and/or unknown. It turns out that telluric contamination is *not* the dominant sources of RV systematic errors in Keck/HIRES data. We later found out that the major culprit behind the RV-BC correlation patterns is probably errors in the DSSTs, which are discussed in Section **??**. This fact makes it somewhat difficult to assess the effectiveness of telluric treatment on real data, but the simulations have demonstrated that the the best and most effective strategy is to have a clean DSST and to forward model the telluric lines (and also to mask out deep lines and de-weight chunks with hard-to-clean tellurics, which are already taken care of by vanking).

Figure 5 represents our best efforts so far and their effects. Our treatment plan includes using "cleaned" DSSTs (we describe how we cleaned the DSSTs later in this subsection) and preliminary modeling of telluric lines in the Doppler code, where we used pwv = 1.0 mm for all observations instead of fitting pwv for each one. In the case of HD 185144, the RV RMS values decreased after we treated the tellurics, but it is not the case for HD 10700 – we suspect that the difference comes from the choice of the pwv value of 1 mm, which is more typical for HD 185144 observations but perhaps not so for HD 10700 (these two stars are at very different Declinations). We plan to model the water absorption in each observation using best-fit or best-estimated pwv in the near future.

How about telluric lines in the DSST? For simulations, we have the privilege of using the synthetic spectrum which is naturally telluric-free. For real observations, telluric contamination enters every observed spectrum associated with the making of DSST (for a detailed description of how the DSST is made, see Appendix? ZZZ To remove errors in the DSST caused by the telluric con-

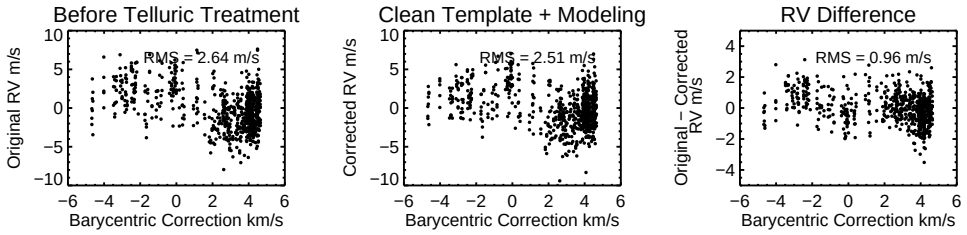

(a) HD 185144, rj82 template

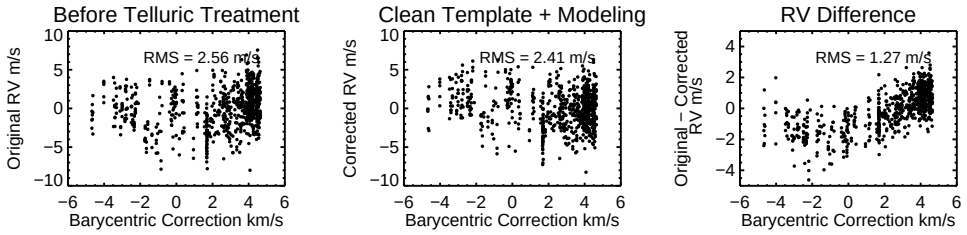

(b) HD 185144, rj172 template

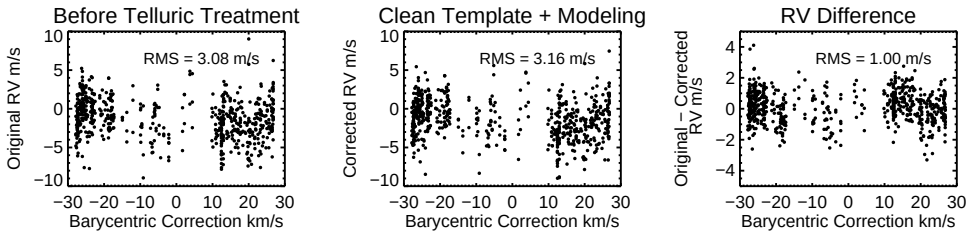

(c) HD 10700, rj82 template

FIG. 5.— Effects of using clean DSST and preliminary telluric modeling on RV precision and accuracy, for HD 185144 (top two rows) and HD 10700 (bottom row). There are two sets of data for HD 185144 because we ran the Doppler code with two DSSTs derived from spectra taken at two different epochs (i.e., at different BCs). The left and middle panels are showing RVs vs. BCs for RV extractions with and without telluric treatment, respectively. The right panels show the RV difference between the two panels.

tamination, we formulated a recipe to "clean up" the DSST:

1. When fitting the bracketing B star + iodine observations, we incorporate synthetic telluric lines generated by TERRASPEC as one of the input reference spectra (just like the iodine atlas). The water column density, or pwv, is determined by fitting two rich water bands among the spectrum taken by the red chip data of Keck/HIRES (7000-8000Å). Although we use Mauna Kea's typical atmospheric condition and adjust oxygen column density according to observation altitude, we still fit for oxygen column density to allow some room for errors in the model (the adjustment needed is typically $<0.5\%$).

2. Using the IPs and wavelength solution derived in step (1), we run the deconvolution algorithm and generate a DSST, which would have telluric lines in it because telluric lines exist in the stellar (iodine-free) spectra.

3. We divide out the telluric lines in the DSST in two steps:

   (a) Fitting two parameters to make sure the telluric lines match the ones in DSST: broadening parameter (width of a Gaussian kernel) and wavelength shift. The broadening parameter is necessary because the synthetic telluric lines are at an extremely high resolution, while the telluric lines in the DSST are deconvolved but are typically lower. The wavelength shift is needed because the wavelengths of the telluric lines, provided by the wavelength solution of the DSST, could differ from rest-frame telluric line wavelengths because of errors in DSST or changing atmospheric conditions such as wind.

   (b) Fitting these two parameters is not a straightforward least-χ^2 problem, because stellar lines are also present in the spectrum and we do not have an input model for them. Thus, instead of minimizing residuals between model (broadened and shifted telluric lines) and data (deconvolved telluric lines plus stellar lines), we minimize the flux above the continuum level to optimize the parameters and the telluric model. In the future, we hope to incorporate this into the code for making DSSTs, i.e., fitting for telluric lines and stellar lines at the same time.

   (c) We divide out the best-fit telluric model from the DSST to obtain a cleaned DSST.

Naturally, this process does not clean up the DSST perfectly, especially for deep and moderately deep lines,

where the line profiles are hard to match. We hope to improve this cleaning process, as well as the entire process for making DSSTs. We plan to run simulations on an M star, HD 95735, also an RV standard. M stars are particularly interesting because they may be more susceptible to telluric contamination – they have more stellar lines in the red where the telluric lines are denser. We also plan to implement full forward-modeling of telluric lines in real data reduction (as opposed to our toy modeling with fixed water column density for all dates/observations), and find out whether a priori or floating water column density parameter works better. We plan to improve the DSST cleaning process by incorporating forward modeling of telluric lines in the "piston Gaussians deconvolver" that is currently used for making DSST, instead of dividing them out. We hope to implement our telluric correction package into the official CPS pipeline eventually, which will be busily processing Keck/HIRES follow-up data on TESS targets (many M dwarfs, undoubtedly) in the near future.

2.5. *Summary of Recommendations on Treating Telluric Contamination*

As argued and tested in the previous subsections, to effectively eliminate the adverse effects of telluric contamination in iodine-calibrated precise RV data, we recommend the following strategies:

- Masking deep and saturated lines and wings liberally, or deserting such spectral regions completely.
- Creating DSST following the recipe described in Section 2.4.1, i.e. modeling "out" telluric lines in every step.
- Incorporating forward modeling of telluric lines in the RV extraction process.
- Assigning low statistical weights to RVs reported by telluric-contaminated spectral regions which suffer from low RV precision and accuracy.

We plan to run simulations on an M star, HD 95735, also an RV standard. M stars are particularly interesting because they may be more susceptible to telluric contamination – they have more stellar lines in the red where the telluric lines are denser. We also plan to implement full forward-modeling of telluric lines in real data reduction (as opposed to our toy modeling with fixed water column density for all dates/observations), and find out whether a priori or floating water column density parameter works better. We plan to improve the DSST cleaning process by incorporating forward modeling of telluric lines in the "piston Gaussians deconvolver" that is currently used for making DSST, instead of dividing them out. We hope to implement our telluric correction package into the official CPS pipeline eventually, which will be busily processing Keck/HIRES follow-up data on TESS targets (many M dwarfs, undoubtedly) in the near future.

The authors thank John A. Johnson for providing a copy of his Doppler code and his help with our incorporation of the code into the HET pipeline. The authors also thank Debra Fischer for her assistance in this regard.

This work was partially supported by funding from the Center for Exoplanets and Habitable Worlds, which is supported by the Pennsylvania State University, the Eberly College of Science, and the Pennsylvania Space Grant Consortium.

The authors appreciate the significant Keck observing time and associated funding support from NASA for the study of long period planets and mulitplanet systems. J.T.W. and S.X.W. acknowledge support from NASA Origins of Solar Systems grant NNX10AI52G.

The work herein is based on observations obtained at the W. M. Keck Observatory, which is operated jointly by the University of California and the California Institute of Technology. The Keck Observatory was made possible by the generous financial support of the W.M. Keck Foundation. We wish to recognize and acknowledge the very significant cultural role and reverence that the summit of Mauna Kea has always had within the indigenous Hawaiian community. We are most fortunate to have the opportunity to conduct observations from this mountain.

The Hobby-Eberly Telescope is a joint project of the University of Texas at Austin, the Pennsylvania State University, Stanford University, Ludwig Maximillians Universität München, and Georg August Universität Göttingen. The HET is named in honor of its principal benefactors, William P. Hobby and Robert E. Eberly.

This work has made use NASA' s Astrophysics Data System Bibliographic Services.

REFERENCES

Artigau, É., Astudillo-Defru, N., Delfosse, X., et al. 2014, in Society of Photo-Optical Instrumentation Engineers (SPIE) Conference Series, Vol. 9149, Society of Photo-Optical Instrumentation Engineers (SPIE) Conference Series, 5
Baranne, A., Queloz, D., Mayor, M., et al. 1996, A&AS, 119, 373
Bean, J. L., Seifahrt, A., Hartman, H., et al. 2010, ApJ, 713, 410
Bender, C. F., Mahadevan, S., Deshpande, R., et al. 2012, ApJ, 751, L31
Bertaux, J. L., Lallement, R., Ferron, S., Boonne, C., & Bodichon, R. 2014, A&A, 564, A46
Butler, R. P., & Marcy, G. W. 1996, ApJ, 464, L153
Butler, R. P., Marcy, G. W., Williams, E., et al. 1996, PASP, 108, 500
Campbell, B., Walker, G. A. H., & Yang, S. 1988, ApJ, 331, 902
Clough, S. A., Iacono, M. J., & Moncet, J.-L. 1992, J. Geophys. Res., 97, 15
Crane, J. D., Shectman, S. A., Butler, R. P., et al. 2010, in Proc. SPIE, Vol. 7735, Ground-based and Airborne Instrumentation for Astronomy III, 773553
Cunha, D., Santos, N. C., Figueira, P., et al. 2014, A&A, 568, A35
Fischer, D. A., Anglada-Escude, G., Arriagada, P., et al. 2016, PASP, 128, 066001
Han, E., Wang, S. X., Wright, J. T., et al. 2014, PASP, 126, 827
Hatzes, A. P., & Cochran, W. D. 1993, ApJ, 413, 339
Latham, D. W., Stefanik, R. P., Mazeh, T., Mayor, M., & Burki, G. 1989, Nature, 339, 38
Marcy, G. W., Isaacson, H., Howard, A. W., et al. 2014, ApJS, 210, 20
Mayor, M., & Queloz, D. 1995, Nature, 378, 355
Mayor, M., Pepe, F., Queloz, D., et al. 2003, The Messenger, 114, 20
Pepe, F., Mayor, M., Galland, F., et al. 2002, A&A, 388, 632

Rothman, L. S., Gordon, I. E., Babikov, Y., et al. 2013, J. Quant. Spec. Radiat. Transf., 130, 4
Sithajan, S., Ge, J., & Wang, J. 2016, in American Astronomical Society Meeting Abstracts, Vol. 227, American Astronomical Society Meeting Abstracts, 137.19
Valenti, J. A., & Fischer, D. A. 2005, ApJS, 159, 141
Valenti, J. A., & Piskunov, N. 1996, A&AS, 118, 595